FINAL REPORT

DE-NE0008429 “Kr/Xe Separation over Metal Organic Framework Membranes”

PI: **Moises A. Carreon**

Chemical and Biological Engineering Department, Colorado School of Mines, Golden, CO 80401

Co-PI: **Praveen Thallapally**

Pacific Northwest National Laboratory, Richland, WA 99352

December 2019

ABSTRACT.

The central thrust of this project is to develop a novel family of continuous membranes, composed of porous crystalline membranes (mainly metal organic frameworks) which offer the possibility of demonstrating high separation performance for Kr/Xe gas mixtures. The specific objectives of the proposed work are: (1) The development of continuous and reproducible MOF membranes on porous tubular supports displaying high Kr permeabilities and high Kr/Xe separation selectivities.(2) Demonstrating the membrane performance long term stability.(3) Establish the basic structure/separation relationships of MOF membranes in Kr/Xe separations, and (4) Demonstrating that membrane synthesis could be amenable to large scale production.

We have demonstrated that porous crystalline molecular sieve membranes including metal organic frameworks, zeolites, and alumino phosphates can effectively separate Kr/Xe gas mixtures ate industrially relevant compositions. Specifically, these three compositions correspond to a different family of microporous crystals, namely zeolites (SAPO-34), metal organic frameworks (ZIF-8) and alumino phosphates (AlPO-18). SAPO-34 membranes displayed the best overall separation performance, while AlPO-18 membranes displayed the highest Kr permeances. The key factors affecting the separation selectivity and permeance of these membranes were identified, and decoupled. The presence of rigid micropores with size lying between Kr and Xe atomic sizes, lower Xe/Kr uptakes (adsorption selectivity), and lower concentration of non-selective pores led to the highest observed Kr/Xe separation selectivities among these three microporous crystals, which corresponded to SAPO-34. The Kr permeances for these three microporous crystalline membrane compositions decreased exponentially with membrane thickness. The best membranes separated Kr/Xe gas mixtures with separation selectivities as high as 45 and Kr permeances ~ as high as 1.2×10^{-7} mol/m^2 s Pa. In addition, SAPO-34 and ZIF-8 membranes were effective in separating Air/Xe mixtures. With separation selectivities as high as 30, and air permeances of 2.3×10^{-7} mol/m^2 s Pa.

Finally, we explore the synthesis in powder form of other potentially suitable porous crystals that if prepared in membrane form could be highly appealing candidates for Kr/Xe and Air/Xe separation. These crystals are porous organic cages which potentially can molecular sieve Kr and air from Xenon based on the unimodal pore sizes lying between the size of the permeant molecules.

RESEARCH DESCRIPTION

1. Introduction.

Krypton and xenon must be captured and separated from spent fuel during reprocessing due to the relatively long half-life of ^{85}Kr (10.8 year), which accounts for 0.2% of the Kr isotopes and decays into rubidium-85. ^{85}Kr emits beta radiation (99.6%) and gamma radiation (0.4%) [1], and direct exposure can harm human health and increase cancer risk [2, 3]. Xenon, however, does not pose the same radiation risks. After a relatively brief period, ^{135}Xe (half-life of 9.2 hours) decays into stable isotope(s) [4]. However, as noble gases, Xe and ^{85}Kr are difficult to separate and must be removed from spent fuel together.

The radioactive ^{85}Kr must be stored for 110 years before atmospheric release [5]. After Xe and ^{85}Kr have been captured, they should be separated. Separating the gases will reduce storage costs since Xe is generally present at 10 times the concentration of Kr and will allow for the economic use of the gases, especially Xe, which has many applications. Separating Kr and Xe will allow for economic use of the gases. Xenon (Xe) is an expensive and important inert gas for many medical and commercial applications. Recovered decontaminated Xe may be used in lighting, electrical, aerospace, and medical applications [6-17]. Xe makes long lived, high intensity light lamps with extremely short flash durations [6]. Commercialized Xe flash lamps have been produced by Sugawara Lab Inc. [6]. Xe is also used in photographic flash lamps [7], arc-lamps in plasma display panels [8] and solar simulation [9], and blue headlights and anti-fog lights on vehicles/as automotive lightings [10]. As an easily-ionized inert gas with high atomic mass and cryogenic storage density, Xe is the most popular propellant used in ion thrusters for satellites in the aerospace field [11]. Xenon is also used as a nontoxic anesthetic [12] and scintillator and ionization-chamber material in X-ray machines for medical imaging applications [13]. Using Xe as a surgical anaesthetic material, with a short induction period, allows for a patient to regain alertness within minutes [14-16]. The value of Xe from spent fuel from a 1000 MW Nuclear plant for 1 year is $281,546 (5,322 grains, $9,050 per metric ton commercially) [17]. Kr captured from off-gases can be used as a radionuclide owing the presence of ^{85}Kr. Kr is used as self-luminescent light sources, and in leak detectors, thickness gauges, and static eliminators [18-21].

However, ^{85}Kr can only be used in limited capacities due to the biological effects of radiation. The value of Kr from spent fuel from 1000 MW Nuclear plant for 1 year is $19,164 (308.18 grains in total, 0.2 % isotope, $616 per metric ton commercially) [17].

Separating Kr from Xe is a challenging task and a highly relevant issue during the treatment of spent nuclear fuel. The physical properties of Kr and Xe are shown in Table 1.1. The current sources of Xe and Kr are very limited, owing to the prevailing separation method. Currently, a ~ 12:1 mixture of Xe and Kr is captured from the liquefaction of air [22]. Cryogenic distillation is also used for separating Kr/Xe in nuclear off-gases. The benchmark technology to separate Kr and Xe is cryogenic distillation process. This method of producing Kr and Xe is extremely energy-intensive, making the products very expensive.

Table 1.1 Physical properties of Krypton and Xenon. [38]

Physical properties	Kr	Xe
Kinetic diameter (nm)	0.366	0.405
Polarizability (10^{-25} cm^3)	24.84	40.44

Membrane separation technology offers a low-energy alternative to separate Krypton from Xenon. It has great potential for applications in industrial separation processes. Kr/Xe separation performance must be improved before membrane separation can be commercially applied to separate the gases. In this application, membranes can exhibit a selectivity of either Kr/Xe (Kr-selective) or Xe/Kr (Xe-selective). In our work, we have focused on Kr-selective membranes.

2. Porous Crystalline Membranes for Kr/Xe Separation

2.1. ZIF-8 membranes for Kr/Xe Separation

We have ddemonstrate that a prototypical type of metal organic framework, zeolitic imidazolate framework-8 (ZIF-8), in membrane form, can effectively separate Kr/Xe gas mixtures at

industrially relevant compositions [23] . The best membranes separated Kr/Xe mixtures with average Kr permeances as high as $1.5 \times 10^{-8} \pm 0.2$ mol/m^2 s Pa and average separation selectivities of 14.2 ± 1.9 for molar feed compositions corresponding to Kr/Xe ratio encountered typically in air. Molecular sieving, competitive adsorption, and differences in diffusivities were identified as the prevailing separation mechanisms. These membranes potentially represent a less-energy-intensive alternative to cryogenic distillation, which is the benchmark technology used to separate this challenging gas mixture. To our best knowledge, this is the first example of any metal organic membrane composition displaying separation ability for Kr/Xe gas mixtures.

This particular MOF has been chosen mainly based on its potential to molecularly sieve Kr over Xe. Based on the kinetic diameter of Kr (~0.37 nm) and Xe (0.41 nm), and the effective aperture size of ZIF-8 in the range of 0.4–0.42 nm, [24], ZIF-8 is an ideal candidate to molecular sieve Kr over Xe. In principle, Kr molecules would diffuse rapidly through the pores, while Xe, at most, will diffuse slowly, meaning that high Kr selectivities could be potentially achieved, based on differences in molecular diffusion.

Porous alumina tubes (Inopor GmbH, inside diameter of 0.7 cm and outside diameter of 1.0 cm, and are asymmetric within the inner layer, which has a pore size of 100 nm) were used as supports to grow ZIF-8 membranes. The support tubes were cut into 10 cm long pieces and glazed on either end. These were calcined at 950 °C for 10 min with heating and cooling rates of 1 °C/min. The supports were left in boiling water for 30 min three times and dried at 150 °C for 8-10 h. The outer surface of the support was wrapped with Teflon tape to prevent membrane growth on the outside surface. The effective permeation area of the support was ~7.5 cm^2. The support and resultant gel were then placed in a stainless-steel autoclave (4713 General Purpose Pressure Vessel, 45 mL, Parr Instrument) and solvothermally treated in a conventional oven at 120 °C for 4-10 hours. The gel covered the supports that were placed vertically in the autoclave. The general approach to prepare ZIF-8 membranes is shown in Figure 2.1.

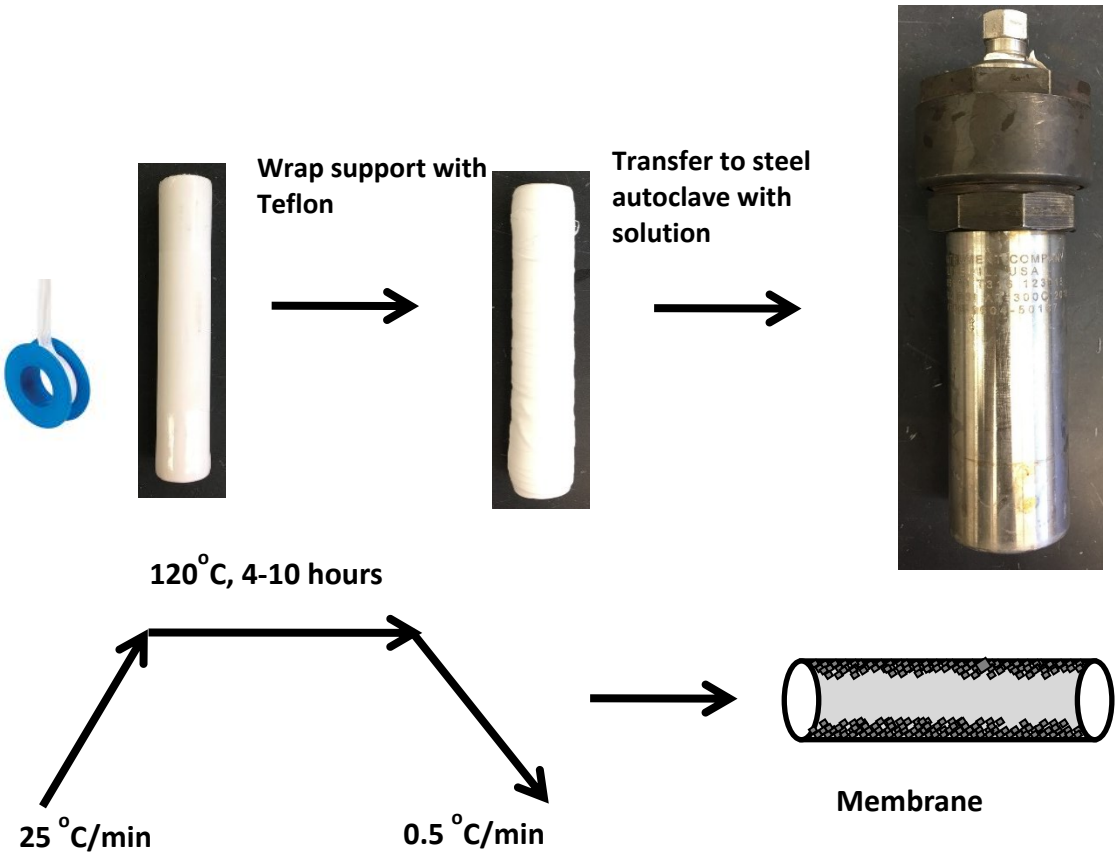

Figure 2.1 General schematic on ZIF-8 membranes preparation process [23]

The synthesized ZIF-8 membranes were used to separate premixed 92:8 Kr/Xe mixtures. This Kr/Xe ratio is close to the typical ratio of these two gases in air. The feed pressure was 223 kPa, and the pressure in the permeate side was 85 kPa. The separation results that were performed at room temperature for these membranes are shown in Table 2.1. Separation selectivities ranged from 5.9- 16.1 depending on membrane synthesis conditions, and number of layers. Kr permenaces ranged from 5.1 to 50.8 GPU. Separation index suggested good membrane reproducibility.

Table 2.1 Kr/Xe Separation Performance over ZIF-8 Membranes. [23]

Membrane ID [a]	Kr permeance (mol/m^2·s·Pa) [b]	Separation selectivity (α)	Separation index (π) [c]
1A	0.33x10^{-8} (9.9)	5.9	13.6 x10^{-4}
1B	0.17x10^{-8} (5.1)	10.8	13.9 x10^{-4}
2A	1.7x10^{-8} (50.8)	12.3	162 x10^{-4}
2B	1.3x10^{-8} (38.8)	16.1	164 x10^{-4}
3	0.5x10^{-8} (14.9)	7.9	28.9 x10^{-4}

Molar gas mixture composition: 92:8 Kr/Xe. Transmembrane pressure 138 kPa. [a] 1A, 1B, 2A,2B are two layer membranes. 3 is three-layer membrane. [b] Numbers in parentheses indicate Gas permeation units (GPU). [c] π= Kr permeance × (selectivity-1) × permeate pressure

Figure 2.2 shows representative SEM images of membranes 1A and 2B. Figure 2.2.a shows the cross-sectional SEM image of membrane 1A, displaying a dense membrane layer with a thickness of ~23 ± 0.8 μm. Membrane 2B (Figure 2.2.c) shows a slightly thinner layer of ~20 ± 1.2 μm. These results are consistent with the separation data shown in Table 2.1. which indicate higher Kr permeance for the thinner membrane 2B. The top-view SEM image for membranes 1A and 2B (Figures 2.1b and 2.1 d, respectively) show well-intergrown and interconnected micrometer-range ZIF-8 crystals. A distinctive morphological feature of the most selective membrane (2B) is the presence of bipyramidal-shaped crystals. This morphology may develop as a result of the different solvothermal history of the membranes. Although we do not understand the potential (if any) role of this morphology in the separation performance, it is well-known that ZIF-8 polycrystalline membrane performance is highly dependent on microstructure.

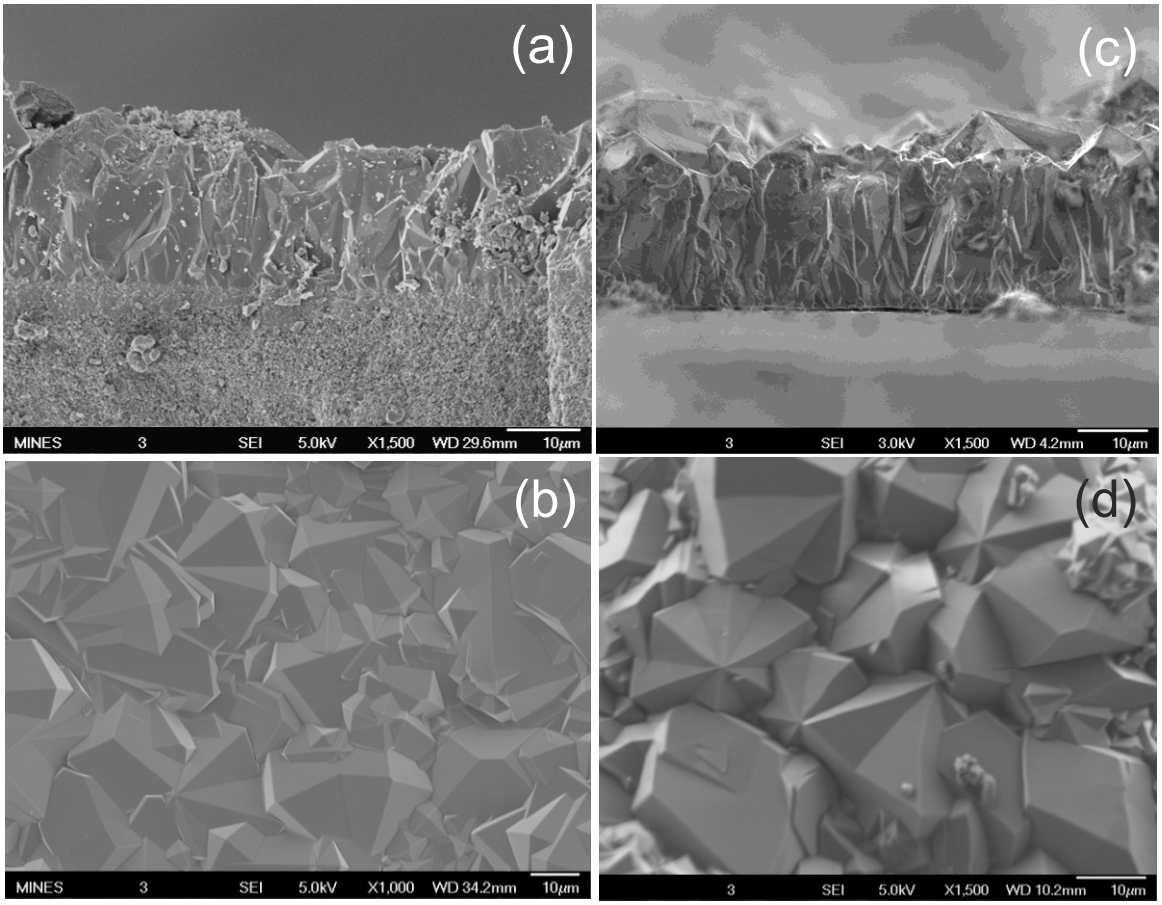

Figure 2.2 SEM images of ZIF-8 membranes: (top row) representative cross section and (bottom row) top view for membrane A1 (panels (a) and (b), respectively) and membrane 2B (panels (c) and (d), respectively). [23]

Three separation mechanisms played an important role for the separation of Kr/Xe gas mixtures over ZIF-8 membranes: *molecular sieving, diffusivity differences, and preferential adsorption*. The separation results showing Kr selective membranes, and the fact that the effective aperture size of ZIF-8 in the range of 0.4–0.42 nm lies approximately between the kinetic diameter of Kr (~0.37 nm) and Xe (~0.41 nm) suggests molecular sieving properties of ZIF-8 membranes for this binary gas mixture. Because of the ZIF-8 flexibility associated with the effective pore size range of 0.4–0.42 nm, sharp molecular sieving effect may be limited. However, based on the observed separation, adsorption, and breakthrough data, molecular sieving plays an important role as separation mechanism. Breakthrough experiments confirmed higher diffusivity of Kr over Xe, favoring again Kr selective membranes. Although adsorption isotherms and isosteric

heat of adsorptions over ZIF-8 crystals suggest that Xe adsorbs more strongly than Kr, Ideal Adsorbed Solution Theory (IAST) predicted that at the prevailing gas separation conditions (Kr/Xe: 92:8 feed composition), Kr/Xe adsorption selectivity was ~4, which also favors Kr selective membranes.

2.2. Other Microporous Crystalline Membranes for Kr/Xe Separation

We have demonstrated the separation ability of another two types of microporous membranes for Kr/Xe gas mixtures. Specifically, we have compared the separation performance of ZIF-8 membranes to the performances of two other types of microporous crystalline membranes: AlPO-18 and SAPO-34. SAPO-34 , a chabazite (CHA) silicoaluminophosphate zeolite displays average pore size of 0.38 nm, which is between the kinetic diameters of Kr (0.37nm) and Xe (0.41nm) [25], and therefore is a highly suitable zeolite to separate Kr from Xe. AlPO-18, a microporous aluminophosphate consisting of $AlPO_4$- and PO_4- tetrahedral units [26]. AlPO-18 exhibits a crystalline structure with AEI topology and a pore size of ~0.38 nm [27], larger than the kinetic diameter of Kr (~0.37 nm) and smaller than that of Xe (~0.41 nm), and therefore, it is a highly suitable candidate to molecular sieve Kr from Xe.

AlPO-18 membranes separated Kr/Xe mixtures with average Kr/Xe separation selectivity of 6.4, and unprecedented high average Kr permeance of 1.6×10^{-7} mol/m^2·s·Pa. Diffusivity difference between Kr and Xe was identified as the dominant separation mechanism.SAPO-34 membranes displayed the best overall separation performance, while AlPO-18 membranes displayed the highest Kr permeances. We identified the key factors affecting both the separation selectivity and permeance. For these three distinctive types of microporous materials, the presence of rigid micropores with size lying between Kr and Xe atomic sizes, lower Xe/Kr uptakes (adsorption selectivity), and lower concentration of non-selective pores led to the highest observed Kr/Xe separation selectivities among these three microporous crystals. The Kr permeances for these three microporous crystalline membranes decreased exponentially as membrane thickness increased.

Secondary seeded growth method was used to prepare AlPO-18 membranes. The synthetic strategy for AlPO-18 membranes is shown in Figure 2.3 . For comparison, the synthesis of ZIF-8

and SAPO-34 membranes is shown too. Membranes were grown on the inside of porous α-Al_2O_3 tubes (Inopor GmbH), having outer and inner diameters of 1.1 cm and 0.7 cm respectively, with an average pore size of 100 nm. Both sides of the tubes were glazed to avoid gas leakage during the membrane gas performance test. The effective membrane area was ~7.5 cm^2. The molar gel composition to prepare AlPO-18 membranes was 1.0 Al_2O_3:1.0 P_2O_5: *x* TEAOH: 200 H_2O (*x* = 1.2, 1.8). Membranes M1 and M2 (Table 2.2.) were prepared with *x* = 1.8. Membranes M3, M4, and M5 (Table 2.2) were prepared with *x* = 1.2. Detailed synthesis conditions are described elsewhere [28].

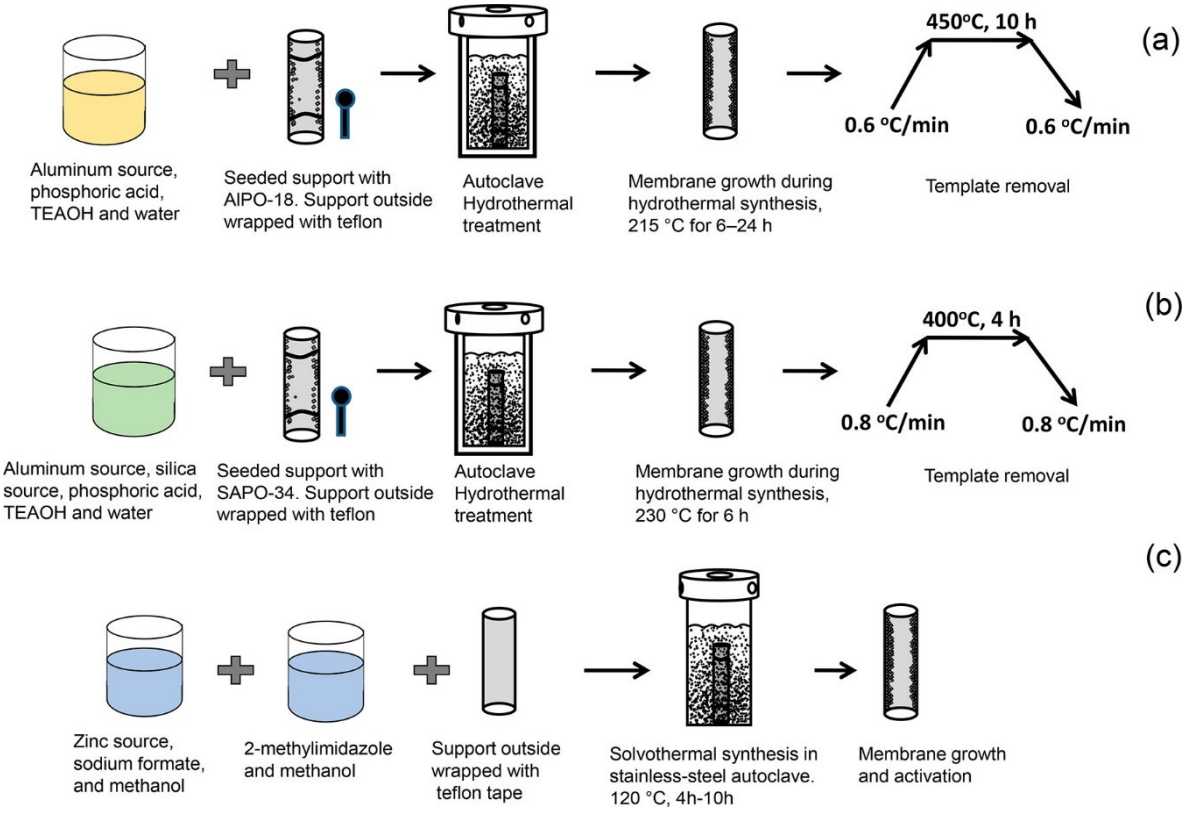

Figure 2.3. General Synthesis Approach for (a) AlPO-18, (b) SAPO-34, and (c) ZIF-8 Membranes [128]

Representative top and cross section view SEM images of AlPO-18 membranes are shown in Figure 2.4. The top view SEM (Figure 2.4a) shows well intergrown rectangular AlPO-18 crystals on the surface of the porous support. Both the membrane crystal size and morphology were different from the original seeds suggesting that the secondary seeded growth promoted heterogeneous nucleation at the support surface and subsequent recrystallization. Specifically,

the crystals size of the membranes was larger than those of the original seeds and the membrane crystals formed rectangular cuboids whereas the seed crystals formed thin hexagonal flakes. The cross-sectional view shows a ~2 μm dense AlPO-18 membrane (Figure 2.4b).

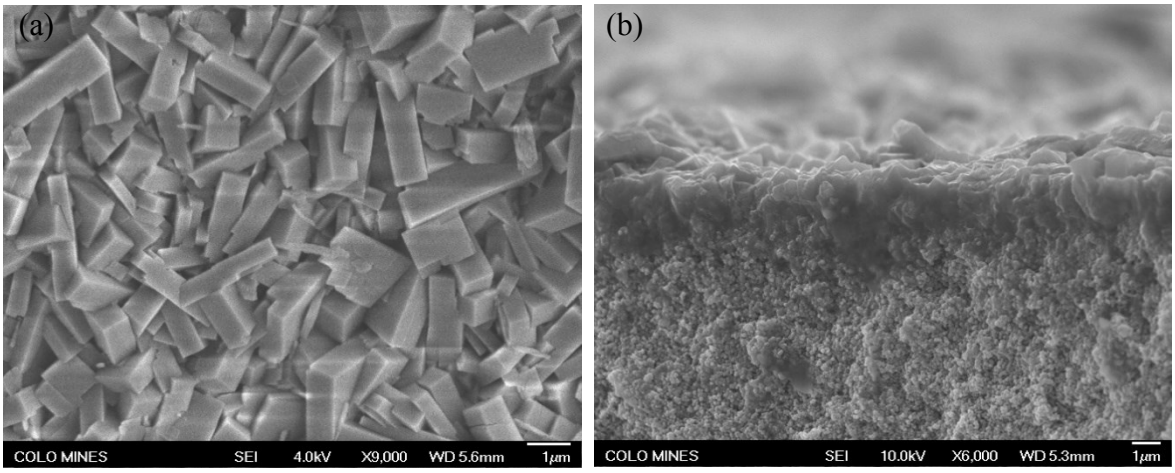

Figure 2.4 (a) Top view and (b) Cross section view SEM images of AlPO-18 membranes [28]

The separation performance of AlPO-18 membranes was evaluated for a premixed 92:8 (molar) Kr/Xe mixture. The feed pressure for the separation experiments was kept constant at 223 kPa, and the pressure in the permeate side was 85 kPa. The separation tests were carried out at room temperature. Table 2.2 summarizes the gas mixture separation results.

Table 2.2 Kr/Xe separation performance over AlPO-18 membranes. Molar feed composition: 92:8 Kr/Xe. Ptransmebrane : 138 kPa. [28] [a] M1-M5 are AlPO-18 membranes, [b] ratio *x* is with respect to Al_2O_3. [c] Numbers in parentheses indicate Gas permeation units (GPU). [d] π= Kr permeance × (selectivity-1) × permeate pressure.

Membrane ID [a]	TEAOH ratio [b] *x*	Membrane Thickness (μm)	Kr permeance x10^{-8} (mol/m^2·s·Pa) [c]	Separation selectivity (α)	Separation index (π)[d] x10^{-2} (mol/m^2·s)
M1	1.8	1.8±0.4	13.7 (409)	4.9	4.5
M2	1.8	1.9±0.3	14.0 (418)	7.5	7.7
M3	1.2	1.9±0.3	31.5 (940)	4.8	10.2
M4	1.2	2.0±0.3	11.6 (346)	7.9	6.8
M5	1.2	2.0±0.3	6.8 (203)	6.8	3.4

The separation performance of our previously reported SAPO-34 [29] and ZIF-8 [23] for Kr/Xe separation vs AlPO-18 membranes is illustrated in Figure 2.5. These results allow a direct comparison between these three distinctive types of microporous crystalline membranes since all these membranes were grown on the same type of porous supports and were evaluated under similar separation conditions. SAPO-34 membranes displayed the best overall separation performance, while ZIF-8 displayed the worst separation performance. SAPO-34 membranes displayed the highest separation index of all three compositions. The reasons for this enhanced separation performance are discussed in the next paragraphs.

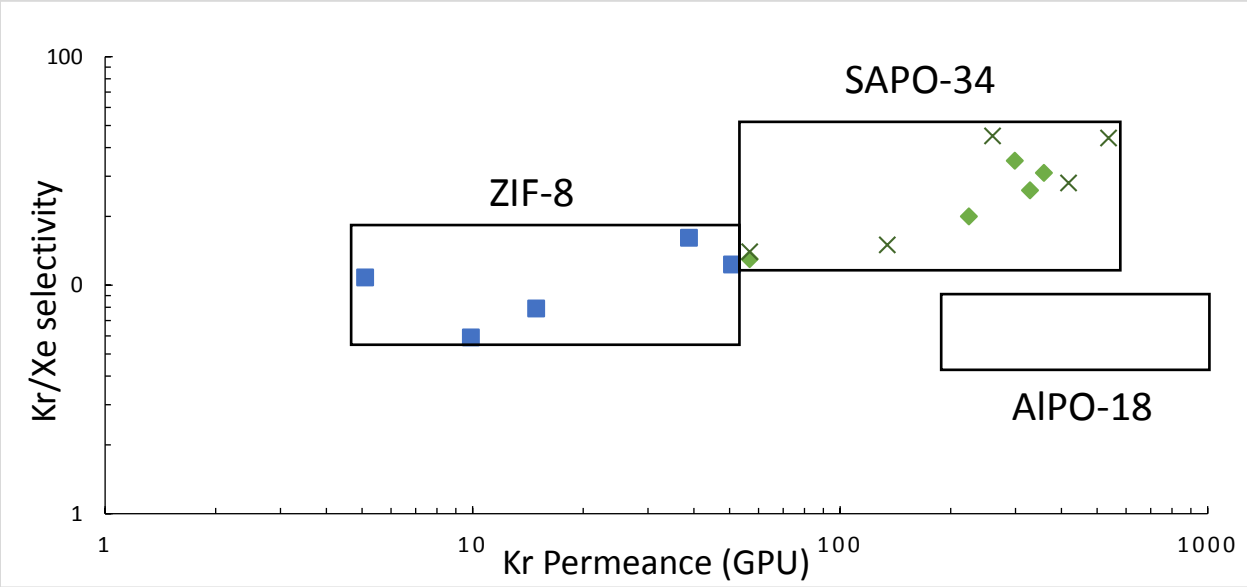

Figure 2.5 Kr/Xe separation selectivity vs Kr permeance over AlPO-18, SAPO-34, and ZIF-8 membranes for a Kr-rich feed gas mixture (molar gas mixture composed of 92:8 Kr/Xe was employed for AlPO-18 (yellow triangles), SAPO-34 (green diamonds) and ZIF-8 (blue rectangles), and 9:1 Kr/Xe molar gas mixture for SAPO-34(green crosses)). [28]

Table 2.3 compares the separation performance of SAPO-34, ZIF-8, and AlPO-18 membranes as a function of average membrane thickness and Kr/ Xe adsorption uptakes. SAPO-34 displayed the highest average Kr/Xe separation selectivity. Two main factors contribute to this enhanced observed selectivity. The first factor is related to the intrinsic molecular sieve property of SAPO-34 imparted by its rigid pore size of 0.38 nm. The second factor is related to the lowest (of the

three membrane compositions) Xe/Kr adsorption selectivity which translates into an attenuated *competitive adsorption* effect, and therefore resulting into higher Kr/Xe separation selectivities.

AlPO-18 membranes displayed the highest average Kr permeances, which can be explained by membrane thickness. AlPO-18 membranes displayed the thinnest layers of all studied membranes. In addition, the highest Kr permeances observed in AlPO-18 membranes can be associated to a higher concentration of *non-selective pathways*. To test this hypothesis, we carried out gas permeation experiments of an equimolar mixture of propane/propylene (kinetic diameters of 0.44nm and 0.42nm respectively) over AlPO-18 and SAPO-34 membranes (both having the same pore size ~0.38 nm). In principle, propane/propylene cannot permeate through the pores (*selective pathway*s) of the microporous crystals, but only through the non-selective pathways. AlPO-18 (M3 and M4) membranes displayed average propane/propylene permeance of 7.2 x 10^{-8} mol/m^2·s·Pa, while SAPO-34 membranes displayed an average propane/propylene permeance of only 2.2 x10^{-8} mol/m^2·s·Pa. These results clearly indicate the presence of a higher concentration of defects (non-selective pathways) for AlPO-18 membranes, leading to higher permeances. This indirect way to quantify defects assumes not significant adsorption effects of propane/propylene over AlPO-18 and SAPO-34.

In addition, these results explain (at least in part) why AlPO-18 membranes displayed lower Kr/Xe separation selectivities as compared to SAPO-34 membranes, despite the fact that both have the same pore size. Another factor that makes AlPO-18 membranes less Kr selective (as compared to SAPO-34) is its high Xe/Kr adsorption selectivity which competes strongly with diffusivity differences, resulting in lower Kr/Xe separation selectivities. The higher Xe adsorption capacity of AlPO-18 over SAPO-34 may be related to the fact that AlPO-18's polarizability strength is higher than SAPO-34's due to the lack of silicon replacing aluminium and phosphate in the pore structure [30]. As compared to AlPO-18 and SAPO-34, ZIF-8 membranes were thicker (~ one order of magnitude) resulting in the lowest Kr permeances. The moderate Kr/Xe separation selectivities observed over ZIF-8 membranes were associated to the flexible nature of its pore structure, limiting its ability to display sharp molecular sieving, and potentially to the presence of defects.

Table 2.3 Separation performance comparison for AlPO-18, SAPO-34 and ZIF-8 membranes [28]. [a] AlPO-18's Kr and Xe adsorption uptakes were collected at 107 kPa and 298K while SAPO-34's and ZIF-8's Kr and Xe adsorption uptakes were at 140 kPa and 298K.

Membrane	Adsorption isotherm [a]				Gas separation performance	
	Xe uptake (cm^3/g)	Kr uptake (cm^3/g)	Xe/Kr adsorption selectivity	Membrane Thickness (μm)	Selectivity (α)	Kr Permeance $x10^{-8}$ ($mol/m^2 \cdot s \cdot Pa$)
SAPO-34	39.9	14.7	2.7	5.1 ± 2.3	25 ± 8.8	8.5± 4.0
ZIF-8	1.7	0.5	3.2	24.7 ± 4.8	10.6 ± 4.0	0.8 ± 0.7
AlPO-18	69	20	3.5	1.9 ± 0.1	6.4 ± 1.5	15.5 ± 9.4

The Kr permeances as a function of membrane thickness for all three membrane compositions is shown in Figure 2.6. The thinner membranes (AlPO-18) displayed Kr permeances ~10–15 times higher than the thickest membranes (ZIF-8). As illustrated by the dashed line on Figure 2.6, the relation between thickness and permeance decreases according to a power function and follows the equation: $P = 4 \times 10^{-7}\, d^{-1.297}$, where d is membrane thickness (μm) and P is Kr permeance ($mol/m^2 \cdot s \cdot Pa$). In principle this correlation may be useful to predict the Kr permeance of other porous crystal compositions with similar micropore sizes of the studied crystals.

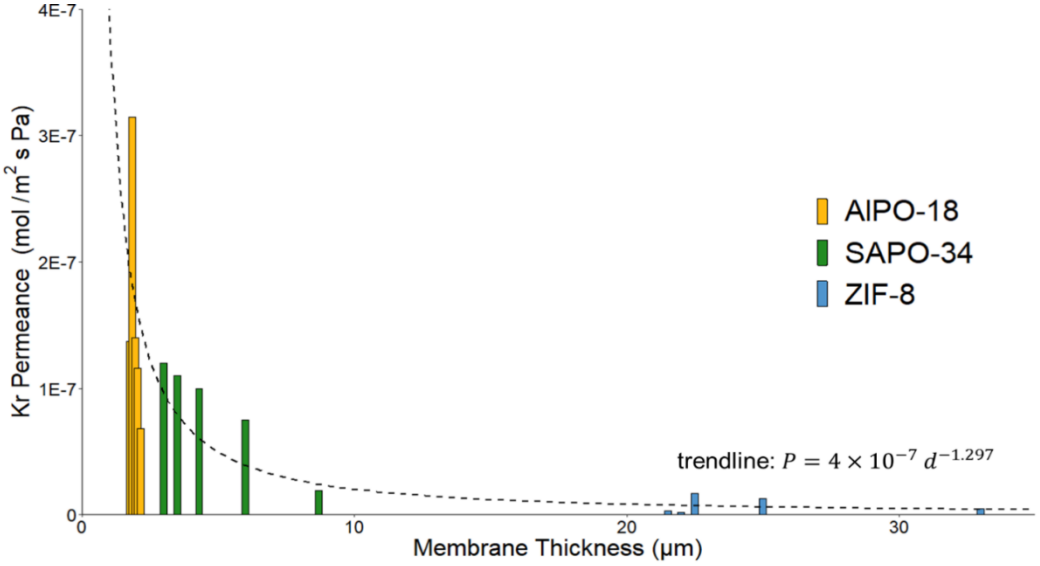

Figure 2.6 Kr permeance for SAPO-34, ZIF-8 and AlPO-18 membranes as a function of membrane thickness over Kr-rich feed gas mixture. The dashed line indicates the fitting equation. [28]

Nair's group reported SAPO-34 membranes applied to Kr and Xe separation with permeability around 50 Barrer and mixture selectivity of 25–30 for Kr at ambient or slightly sub-ambient conditions [31]. Later on, the same research group reduced membrane thickness and applied ion exchange with alkali metal cations to improve performance [32]. Kr permeance improved from 7.5 to 26.3 gas permeation units (GPU) while ideal Kr/Xe selectivities exceeded 20 at 298 K. Selectivity in cation-exchanged membranes significantly increased (> 50%) under ambient and slightly subambient conditions [32].

Grand canonical Monte Carlo and biased molecular dynamics simulations support our experimental findings on the nature of adsorption- and diffusion-based Kr/Xe separation mechanisms over SAPO-34, and ZIF-8 [33]. Xenon is found to preferentially adsorb on all materials, but diffusion selectivity for krypton is found to dominate the overall membrane separation selectivity [33]. The rigid SAPO-34 framework was more effective at excluding xenon than the more flexible ZIF-8. Indeed, during xenon "window crossing," the SAPO-34 window opened to only 3.8 Å, while the ZIF-8 window opened to 4.1 Å, resulting in a lower free energy "diffusion" barrier for xenon in ZIF-8. Therefore, an ideal membrane material for Kr/Xe separation should be rigid and have large pore cages and small pore windows [33].

2.3. Microporous Crystalline Membranes for Xe Separation from air

ZIF-8 is a suitable candidate to molecular sieve air (N_2, O_2, CO_2 and Ar) over Xe. Our gropu has demonstrated that continuous ZIF-8 membranes can effectively separate air/Xe gas mixtures [34]. These membranes showed air permeances as high as 3.94 x 10^{-8} mol/m^2 s Pa and separation selectivities as high as 12.4 for air/Xe molar feed composition of 9:1. These membranes separated air from Xe via molecular sieving, preferential adsorption, and diffusivity differences. Membranes were air selective, suggesting that both molecular sieving and diffusivity differences were the dominant separation mechanisms. The proposed membrane technology may be an attractive separation approach to recover Xe from air mixtures.

The separation performance of ZIF-8 membranes prepared in this study was evaluated using premixed air/Xe gas mixtures with molar ratio of 90:10. The feed and permeate pressures were kept at 223 kPa and 85 kPa, respectively. The separation data for three ZIF-8 membranes is shown in Table 2.4. M1 and M2 displayed permeances of 3.1 and 3.9×10^{-8} mol/m^{2}sPa and air/Xe separation selectivities of 11.3 and 12.4. Membrane M3 was prepared by adding an extra ZIF-8 layer to a membrane prepared with identical gel compositions and solvothermal synthesis conditions as those of M1 to form a 3-layer membrane. Separation selectivity decreased compared to those of the 2-layer membranes (M1 and M2). The reduction in separation selectivity may be associated with an increase in the concentration of defects and/or non-selective pore pathways.

Membrane separation indexes ranged between 2.1 $\times 10^{-2}$ and 3.8×10^{-2} respectively, indicating good membrane reproducibility.Continuous ZIF-8 membranes are demonstrated to effectively separate air/Xe gas mixtures. These membranes showed air permeances as high as 3.94×10^{-8} mol/m^2 s Pa and separation selectivities as high as 12.4 for air/Xe molar feed composition of 9:1. These membranes separated air from Xe *via* molecular sieving, preferential adsorption, and diffusivity differences. Membranes were air selective, suggesting that both molecular sieving and diffusivity differences were the dominant separation mechanisms. The proposed membrane technology may be an attractive separation approach to recover Xe from air mixtures. To our best knowledge, this work represents the first known example of any membrane composition displaying separation ability for air/Xe gas mixtures.

Table 2.4 Air (N_2 and O_2) /Xe separation performance over ZIF-8 membranes at room temperature; molar gas mixture composition: 90:10 air/Xe; transmembrane pressure: 138 kPa; feed flow rate: 40 ml/min. In parenthesis for the air permeance include GPU and mention as footnote that numbers in parenthesis indicate GPUs. [34]

Membrane ID	Air permeance $\times 10^{-8}$ (mol/m^2·s·Pa) (GPU)	Separation selectivity (α)	Separation index (π) $\times 10^{-2}$
M1	3.10 (92.6)	11.3	2.7
M2	3.94 (117.7)	12.4	3.8
M3	3.94 (117.7)	7.4	2.1

Representative SEM images of membranes M1–M3 are shown in Figure 2.7. Top view SEM images of M1–M3 (Figures 2.7 (a), (c) & (e)) show well-intergrown and interconnected micron-range ZIF-8 crystals. A distinctive morphological feature of membranes M1, M2 and M3 is the presence of pyramidal-shaped crystals. This morphology may have resulted from the membrane different solvothermal histories.

In general, membranes M1 and M2 show smaller crystal aggregates sized up to ~33 μm as compared to M3, which contains aggregates sized up to ~68 μm. M3's larger crystal aggregates may have grown during the recrystallization process upon the addition of the third layer. The cross-sectional image of membrane M1, shown in Figure 2.7 (b), displays a dense membrane layer with thickness of ~13±3 μm. M2 shows a slightly thicker layer of ~14±2 μm as shown in Figure 2.7(d). M3 displayed a thickness of 27±6 μm (Figure 2.7(e)). M2 and M3 displayed higher air permeance than M1. Since these two membranes are thicker than M1, this suggests that their higher permeance may be related to a higher concentration of defects. It is common that ZIF-8 polycrystalline membrane performance is highly dependent on microstructure characteristics, including morphology, crystal size, thickness, intergrowth, defects, and gaps or cracks.

Molecular sieving and *differences in diffusivities* were the two main separation mechanisms which contributed to the observed air over Xe selective membranes. The effective aperture size of ZIF-8 (~0.4-0.42 nm), lying between the kinetic diameters of N_2 and O_2 (0.36 nm, and 0.35 nm) and Xe (~0.41 nm), suggests potential molecular sieving properties of ZIF-8 membranes for this gas mixture. Estimation of Fickian diffusivities indicate that air diffuses faster than Xe promoting the separation via differences in diffusivities. On the other hand, the observed Xe/air *preferential adsorption selectivity* competes strongly against molecular sieving and diffusivity differences. Nevertheless, the observed air/Xe separation selectivities indicate that molecular sieving and differences in diffusivities were the two dominant separation mechanisms.

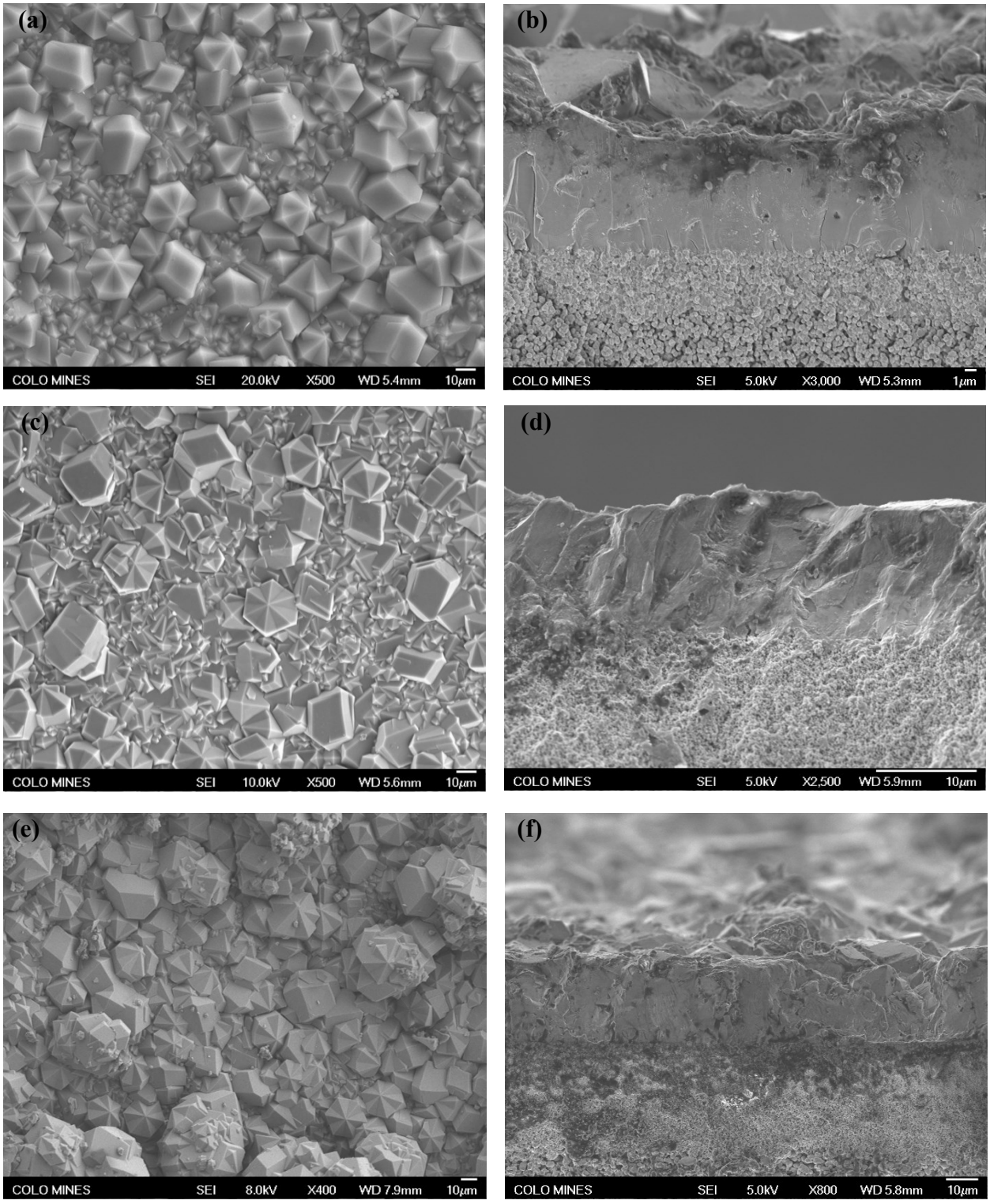

Figure 2.7 Representative cross section and top view SEM images of ZIF-8 membranes: (a) and (b) for membrane M1; (c) and (d) for membrane M2; (e) and (f) for membrane M3. [34]

SAPO-34 membranes are highly suitable to separate xenon from air. Our group demonstrated that continuous SAPO-34 membranes exhibit enhanced performance separating air/Xe gas mixtures [35]. Specifically, SAPO-34 membranes showed air permeances as high as 2.3 x 10^{-7} mol/m^2 s Pa (690 GPU) and separation selectivities as high as 30.1 for a molar feed of 9:1 air/Xe. Molecular sieving, competitive adsorption, and diffusivity differences played a critical role in the overall separation performance. Membranes were air selective due to favorable molecular sieving and differences in diffusivity between gases present in the air mixture and Xe. Molecular sieving and diffusivity differences were identified as the dominant separation mechanisms.

Table 2.5 summarizes the separation results of four SAPO-34 membranes for air/Xe molar feed composition of 9:1. The studied feed molar composition is a representative composition found typically in nuclear reprocessing plants. The composition of air was 79% N_2 and 21 % O_2. Four membranes denoted as M1-M4 were synthesized independently via secondary seeded growth (see Experimental section). M1-M4 displayed air permeances in the 97-690 GPU range and air/Xe separation selectivities of 7.1-31.1. As shown in Table 2.5, the highest air permeable membrane (M3) displayed the lowest separation selectivity, while the most selective membranes (M1 and M2) showed the lowest air permeances. These observations adhere to the typical trend of selectivity-permeance trade-off for membranes. The separation index π for all membranes ranged from 7.6-25.7x10^{-2} mol·m-^{2}·s-^{1}, indicating reasonable membrane reproducibility.

Table 2.5 Air/Xe separation performance over SAPO-34 membranes at room temperature; molar gas mixture composition: 90:10 air/Xe; transmembrane pressure: 138 kPa; feed flow rate: 40 ml/min. [a] Refers to Air (O_2+N_2)/Xe [35]

Membrane ID	Air permeance x10^{-8} (mol·$m^{-2}s^{-1}$Pa) (GPU)	Separation selectivity (α) [a]	Separation index (π) x10^{-2} (mol·$m^{-2}s^{-1}$)
M1	5.4 (161)	30.1	13.4
M2	3.2 (97)	28.6	7.6
M3	23.1 (690)	14.1	25.7
M4	14.6 (436)	21.6	25.6

Figure 2.8 shows the top views and cross views of M1 and M3. The top view images (Fig. 2.8a and 2.8c) show well-intergrown rectangular SAPO-34 crystals on the surface of the 100 nm

alumina porous supports. The size of the surface crystals of the membranes was larger than the crystal size of the seeds, suggesting that secondary seed growth led to a recrystallization process.

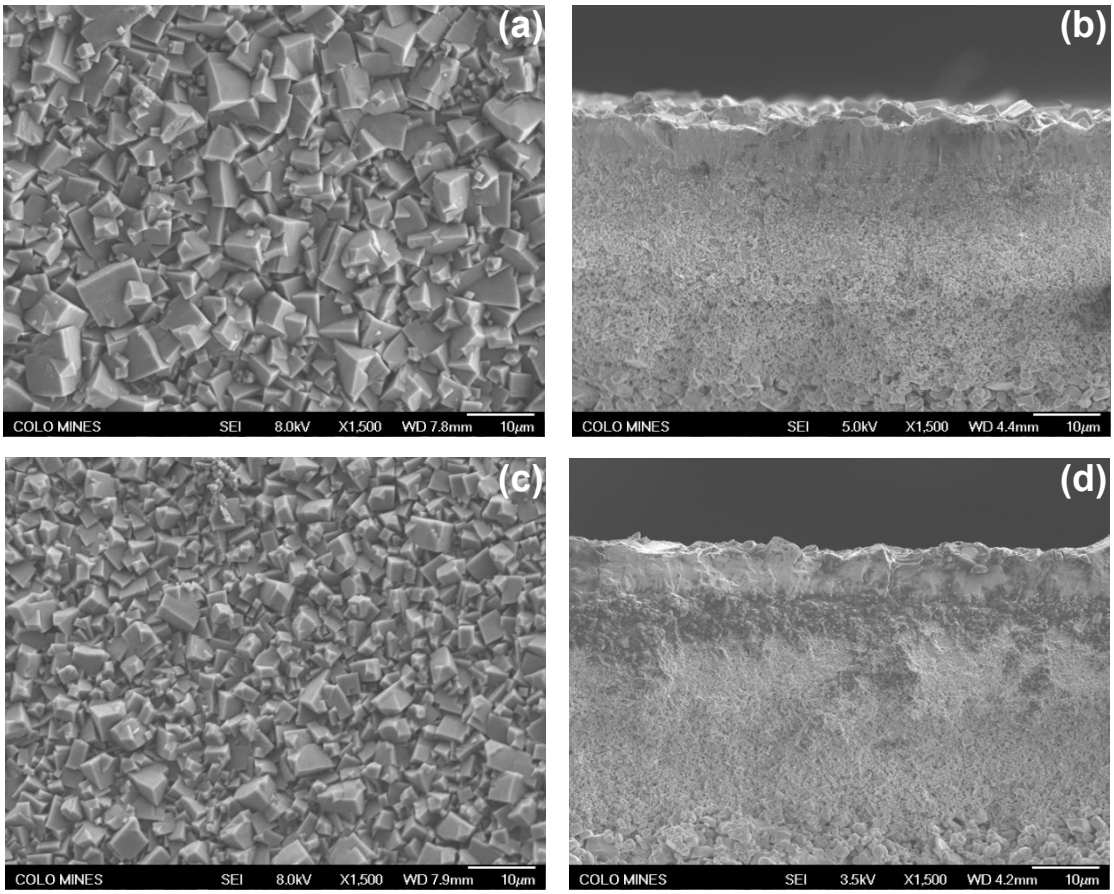

Figure 2.8 (a,c) Representative top views and (b,d) Representative cross section views SEM images of SAPO-34 membranes M1 and M3 [35]

The crystal sizes of membrane M1 were slightly larger than those of membrane M3. Specifically, the M1 crystal sizes ranged from ~1.1-2.9 μm to 4.3-9.8 μm, while those of M3 surface crystals ranged from 0.6-1.3 μm to 2.2-6.0 μm. In principle, small crystals generally pack better than larger crystals, potentially leading to less defective membranes. Interestingly, M1 (displaying larger surface crystals) led to higher separation selectivity as compared to M3. This may be rationalized by a lower concentration of grain boundaries and thus a higher concentration of selective (pore) pathways. Therefore, it is likely that along with smaller crystals, the M1 membrane had more defects and/or non-

selective pathways. The cross-sectional views for M1 and M3 (Fig. 2.8b and 2.8d) show membrane layers with thicknesses of ~6.2 μm and ~6.4 μm, respectively. Since the thicknesses of both membranes are comparable, the higher air permeance observed for M3 indicates a more defective membrane.

In Figure 2.9, we compare the separation performance of SAPO-34 vs ZIF-8 membranes. This Figure allows for a direct comparison between these two distinctive types of microporous crystalline membranes since both types of membranes were grown on the same type of porous supports and were tested under similar separation conditions. Overall, SAPO-34 membranes displayed higher permeance and higher separation selectivity.

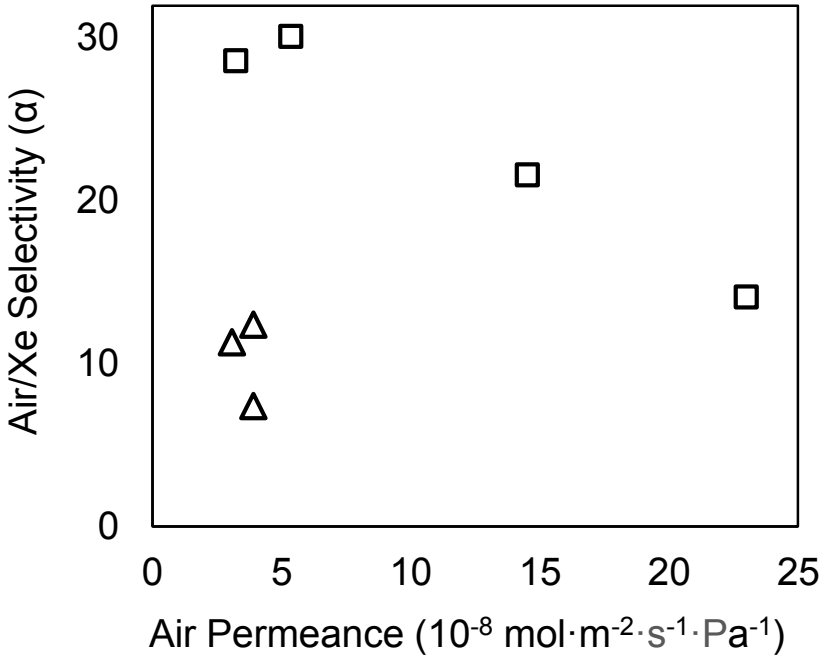

Figure 2.9 Air/Xe separation selectivity vs Kr permeance over SAPO-34 (□), and ZIF-8 (△) membranes for a 9:1 air/Xe molar gas mixture. [35]

Table 2.6 shows the average separation performance of both types of membranes. SAPO-34 displayed separation selectivities more than two times higher than those observed for ZIF-8 membranes. The main factor contributing to the higher observed separation selectivities for SAPO-34 membranes is the intrinsic molecular sieve property of SAPO-34 determined by its *smaller rigid pore size* of 0.38 nm as compared to ZIF-8's larger adjustable pore size (0.40-

0.42nm). This observation is supported by recent molecular simulation studies on SAPO-34 and ZIF-8 membranes which demonstrate that the rigid SAPO-34 framework was more effective at excluding Xe than ZIF-8. [33] Specifically, it was found that there is a higher energy diffusion barrier for Xe over SAPO-34 (as compared to ZIF-8). [33] Therefore, the stiffer SAPO-34 windows promote a more effective molecular sieving, leading to a higher separation selectivity. It is important to mention, that while simulations suggest that SAPO-34 is close to exhibiting true molecular sieving, it still allows Xe to penetrate through its pores, albeit infrequently. Also, SAPO-34 membranes displayed more than 3 times higher average air permeances as compared to ZIF-8 membranes. Air permeance correlates with membrane thickness. It is important to mention that SAPO-34 membranes may be sensitive to moisture, and therefore its separation performance may be compromised in the presence of water. Therefore a dry air-Xe feed is highly desirable for effective separation.

Table 2.6 Average air/Xe Separation performance comparison for SAPO-34 and ZIF-8 [35].

	Average	Average gas separation performance		
Membrane Composition	membrane Thickness (μm)	Selectivity (α)	Air permeance (GPU)	Separation index (π) x10^{-2}
SAPO-34	6.3	23.6	346	18.1
ZIF-8	18	10.4	109	2.9

Overall, the studied microporous crystals in membrane form are highly appealing to effectively separate Kr/Xe and air/Xe gas mixtures. Other functional microporous crystals including porous organic cages (POCs) [36,37] may be highly suitable for these separations if prepared in membrane form. Recently, our group has reported the successfully synthesis of prototypical types of porous organic cages via conventional [38,39], and novel approaches [40,41]. These crystals are highly appealing to be used as "seeds" for the development of continuous POC membranes.

2.4. Long Term Stability Studies

We evaluated the long term stability of two microporous crystalline membranes: ZIF-8 and SAPO-34 for Kr/Xe mixtures, and Air/Xe mixtures. We found that both membrane compositions SAPO-34 and ZIF-8 are stable at least up to 2-3 months. Specifically, both membrane compositions retain their separation performance after been tested for 8-12 weeks. In the case of SAPO-34 the overall separation performance (considering both selectivity and permeance) decreased only ~5-6 %, while for ZIF-8 decreased by ~12-15%. The larger decrease in separation performance for ZIF-8 membranes is mainly related due to the flexible nature of this MOF imparted by its organic linker.

Air/Xe separation.

Tables 2.7 and 2.8 summarize the separation performance for SAPO-34 and ZIF-8 membranes for Air/Xe separation respectively . Membranes were evaluated after 2 and 3 months for SAPO-34 and 2 months for ZIF-8.

Table 2.7. Air/Xe separation performance over SAPO-34 membranes at room temperature; molar gas mixture composition: 90:10 air/Xe; transmembrane pressure: 138 kPa; feed flow rate: 40 ml/min. [a] Refers to Air (O_2+N_2)/Xe

Membrane ID	Air permeance x10^{-8} (mol·$m^{-2}s^{-1}$Pa)	Separation selectivity (α) [a]
M1	5.4	30.1
M2	3.2	28.6
M3	23.1	14.1
M4	14.6	21.6

Membrane stability was evaluated after 2 and 3 months, and results are shown in Table 2.7a and Table 2.7b respectively.

Table 2.7a. Air/Xe separation performance over SAPO-34 membranes at room temperature; molar gas mixture composition: 90:10 air/Xe; transmembrane pressure: 138 kPa; feed flow rate: 40 ml/min. [a] Refers to Air (O_2+N_2)/Xe. Membranes tested after 2 months. Only most selective membranes were evaluated.

Membrane ID	Air permeance x10^{-8} (mol·$m^{-2}s^{-1}$Pa)	Separation selectivity (α) [a]
M1	5.1	31.2
M2	3.0	29.1
M3	N/A	N/A
M4	N/A	N/A

Table 2.7b Air/Xe separation performance over SAPO-34 membranes at room temperature; molar gas mixture composition: 90:10 air/Xe; transmembrane pressure: 138 kPa; feed flow rate: 40 ml/min. [a] Refers to Air (O_2+N_2)/Xe. Membranes tested after 3 months. Only most selective membranes were evaluated.

Membrane ID	Air permeance x10^{-8} (mol·$m^{-2}s^{-1}$Pa)	Separation selectivity (α) [a]
M1	5.0	30.9
M2	3.1	29.3
M3	N/A	N/A
M4	N/A	N/A

Table 2.8 Air (N_2 and O_2) /Xe separation performance over ZIF-8 membranes at room temperature; molar gas mixture composition: 9:1 air/Xe; transmembrane pressure: 138 kPa; feed flow rate: 40 ml/min.

Membrane ID	Air permeance x10^{-8} (mol/m2·s·Pa)	Separation selectivity (α)
M1	3.10	11.3
M2	3.94	12.4
M3	3.94	7.4

Membrane stability was evaluated after 2 months only, and results are shown in Table 2.8a .

Table 2.8a Air (N_2 and O_2) /Xe separation performance over ZIF-8 membranes at room temperature; molar gas mixture composition: 9:1 air/Xe; transmembrane pressure: 138 kPa; feed flow rate: 40 ml/min. Membranes tested after 2 months. Only two membranes were evaluated (most selective).

Membrane ID	Air permeance $x10^{-8}$ (mol/m2·s·Pa)	Separation selectivity (α)
M1	2.70	11.3
M2	3.30	12.6
M3	N/A	N/A

Kr/Xe separation.

SAPO-34 membranes.

We evaluated the long term stability of one SAPO-34 membrane after 2, and 3 months. An original membrane separated Kr/Xe mixtures with Kr permeance of 1.0×10^{-7} mol/m^2 s Pa and separation selectivity of 35. The separation conditions were: Molar gas mixture composition: 9:1 Kr/Xe. Transmembrane pressure: 138 kPa. Table 2.9 shows the separation data after 2 and 3 months under similar separation conditions as the original membrane.

Table 2.9 Kr/Xe Separation Performance over SAPO-34 Membrane. Long term stability.

Stability	Kr permeance $x10^{-7}$ (mol·m^{-2}s^{-1}Pa)	Separation selectivity (α)
2 months	0.92	36.2
3 months	0.90	35.4

ZIF-8 membranes.

We evaluated the long term stability of one ZIF-8 membrane after 2, and 3 months. An original membrane separated Kr/Xe mixtures with Kr permeance of 1.3×10^{-8} mol/m^2 s Pa and separation selectivity of 16.1. The separation conditions were: Molar gas mixture composition: 92:8 Kr/Xe. Transmembrane pressure: 138 kPa. Table 2.10 shows the separation data after 2 and 3 months under similar separation conditions as the original membrane.

Table 2.10 Kr/Xe Separation Performance over ZIF-8 Membrane. Long term stability.

Stability	Kr permeance $x10^{-8}$ ($mol \cdot m^{-2}s^{-1}Pa$)	Separation selectivity (α)
2 months	1.1	16.4
3 months	1.0	16.3

2.5. Scale-up Studies

We attempted to synthesize ZIF-8 membranes on 25 cm long alumina porous supports and did single gas permeation experiments with helium to assess if the membranes were continuous. None of the membranes that we synthesized hold pressure while permeating helium. This indicates that the membranes were highly defective and therefore unselective for any gas mixture. Therefore, the resultant membranes were not evaluated for Kr/Xe or Air/Xe gas mixtures. We added multiple layers (up to 7) to heal membrane defects, and potentially get a continuous membrane, However, the strategy did not work. Further work is needed to achieve this goal. Scale-up membranes is quite challenging, and only very few literature exists on scaling up porous crystalline membranes [42].

In summary, we demonstrated the successful synthesis of continuous and reproducible microporous crystalline membranes including MOF membranes displaying high Kr permeabilities and high Kr/Xe separation selectivities at industrially relevant feed compositions. The resultant membranes were also effective in separating air from xenon mixtures. We demonstrated the membrane performance long term stability, and establish basic structure/separation relationships of these membranes for Kr/Xe and air/Xe mixtures. Three main separation mechanisms were found to play a role in the overall separation performance of the membranes: *molecular sieving*, *differences in diffusivities*, and *competitive adsorption*. Membrane scale-up was challenging, nevertheless initial attempts to synthesize MOF membranes on large porous tubes were made.

PUBLICATIONS

The following publications resulted from this project:

1) J. M. Lucero, J. B. Jasinski, M. Song, D. Li, L. Liu, J. Liu, J. De Yoreo, P. K. Thallapally, M. A. Carreon, Synthesis of Porous Organic Cage CC3 via Solvent Modulated Evaporation, ***Inorganica Chimica Acta*** **2019**, in press, DOI: 10.1016/j.ica.2019.119312.

2) J. Lucero, J.M. Crawford, C. Osuna, M.A. Carreon, Solvothermal synthesis of porous organic cage CC3 in the presence of dimethylformamide as solvent, ***CrystEngComm*** **2019**, 21, 34, 5039-5044.

3) T. Wu, J. Lucero, J.M. Crawford, M.A. Sinnwell, P.K. Thallapally, M.A. Carreon, SAPO-34 Membranes for Xenon Capture from Air, ***Journal of Membrane Science*** **2019**, 573, 288-292.

4) T. Wu, J. Lucero, M.A. Sinnwell, P.K. Thallapally, M.A. Carreon, Recovery of Xenon from air over ZIF-8 membranes, ***Chemical Communications*** **2018**, 54, 8976-8979.

5) T. Wu, J. Lucero, Z. Zong, S.K. Elsaidi, P.K. Thallapally, M.A. Carreon, "Microporous crystalline membranes for Kr/Xe Separation: Comparison between AlPO-18, SAPO-34, and ZIF-8", ***ACS Applied Nano Materials*** **2018**, 1, 463-470.

6) R. Anderson, B. Schweitzer, T. Wu, M.A. Carreon, D. Gomez-Gualdron, "Molecular simulation insights on Xe/Kr separation in a set of nanoporous crystalline membranes" ***ACS Applied Materials & Interfaces*** **2018,** 10, 582-592.

7) J. Lucero, S.K. Elsaidi, R. Anderson, T. Wu, D. Gomez Gualdron, P.K. Thallapally, M.A. Carreon, "Time Dependent Structural Evolution of Porous Organic Cage CC3", ***Crystal Growth & Design*** **2018**, 18, 2, 921-927.

8) T. Wu, X. Feng, S. K. Elsaidi, P.K. Thallapally, M. A. Carreon, Zeolitic Imidazolate Framework-8 (ZIF-8) membranes for Kr/Xe separation, ***Industrial & Engineering Chemistry Research*** **2017**, 56, 1682–1686.

9) X. Feng, Z. Zong, S. K. Elsaidi, J. B. Jasinski, R. Krishna, P.K. Thallapally, M. A. Carreon, "Kr/Xe Separation over a Chabazite Zeolite Membrane" ***Journal of the American Chemical Society*** **2016**, 138, 31,9791–9794.

FINAL QUAD CHART

U.S. DEPARTMENT OF ENERGY
Nuclear Energy

Kr/Xe separation over Metal Organic Framework Membranes

OVERVIEW

Purpose: Summary statement of project purpose
The central thrust of this proposal is to establish a solid fundamental science program leading to the rational design of a novel family of membranes, composed of metal organic frameworks which offer the possibility of demonstrating high separation performance for Kr/Xe gas mixtures.

Objectives: Bulleted list of summarized objectives
(1) The development of continuous and reproducible MOF membranes on porous tubular supports displaying high Kr permeabilities and high Kr/Xe separation selectivities.
(2) Demonstrating the membrane performance long term stability.
(3) Establish the basic structure/separation relationships of MOF membranes in Kr/Xe separations.
(4) Demonstrating that membrane synthesis could be amenable to large scale production.

IMPACT

Logical Path: Description (or flowchart) of logical path to accomplish work
We propose to develop continuous and robust type of membranes, composed of metal organic frameworks (MOF), which show great promise for Kr/Xe separation. The particular MOF compositions have been chosen based on two important criteria: (1) limiting pore aperture (or window openings) and/or (2) Differences in adsorption capacities. Membranes will be characterized and evaluated for Kr/Xe gas mixtures at various feed compositions, feed pressures and temperatures.
Outcomes: Brief summary of expected project outcomes
If successful, the proposed research will result in the development of novel membranes capable of effectively separating Kr from Xe with high flux and selectivity. The ability to fabricate thin, chemically and mechanically stable MOF membranes for nuclear gas treatment constitutes an important new direction in membrane science with the goal of achieving higher combinations of selectivity and permeability overcoming current conventional fractional distillation approach. This research may result in the development of robust membranes, as a viable energy saving approach for the effective removal of 85Kr during processing of spent nuclear fuel.

DETAILS

Principal Investigator: Moises A. Carreon

Institution: Colorado School of Mines. Chemical & Biological Engineering Dept.

Collaborators: Praveen Thallapally (PNNL)

Duration: 36 months **Total Funding Level:** $ 375,000

TPOC: Bob Jubin

Federal Manager: Jim Bresee

Workscope: FC-1.2: Materials Recovery

PICSNE Workpackage #: NU-15-CO-CSM-0201-01

RESULTS

1. We demonstrated the successful synthesis of continuous and reproducible microporous crystalline membranes including MOF membranes displaying high Kr permeabilities and high Kr/Xe separation selectivities at industrially relevant feed compositions. The resultant membranes were also effective in separating air from xenon mixtures. We demonstrated the membrane performance long term stability, and establish basic structure/separation relationships of these membranes for Kr/Xe and air/Xe mixtures. Three main separation mechanisms were found to play a role in the overall separation performance of the membranes: molecular sieving, differences in diffusivities, and competitive adsorption. Membrane scale-up was challenging, nevertheless initial attempts to synthesize MOF membranes on large porous tubes were made.

References

1. Abe, K., Hosaka, J., Iida, T., Ikeda, M., Kobayashi, K., Koshio, Y., ... & Nakajima, Y. (2009). Distillation of liquid xenon to remove krypton. Astroparticle Physics, 31(4), 290-296.

2. NCRP Report 44: Krypton-85 In The Atmosphere-Accumulation, Biological Significance, and Control Technology. Washington, DC, NCRP, 1975

3. NCRP Report: Krypton-85 In The Atmosphere-With Specific Reference to the Public Health Significance of the Proposed Controlled Release at Three Mile Island. Washington, DC, NCRP, 1980

4. Nuclear Power: What is Xenon https://www.nuclear-power.net/nuclear-power/reactor-physics/reactor-operation/xenon-135/?pdf=18603

5. Gombert, D., Ebert, W., Marra, J., Jubin, R., & Vienna, J. (2008). Global nuclear energy partnership waste treatment baseline. Papers, 235th ACS Nat. Meet., New Orleans, LA (the United States).

6. Sugawara Laboratories Inc. – Xenon Flashlamps http://www.sugawara-labs.co.jp/en/xenonflashes/xenon

7. Wekhof, A. (2000). Disinfection with flash lamps. PDA Journal of Pharmaceutical Science and Technology, 54(3), 264-276.

8. Kim, C. H., Kwon, I. E., Park, C. H., Hwang, Y. J., Bae, H. S., Yu, B. Y., ... & Hong, G. Y. (2000). Phosphors for plasma display panels. Journal of Alloys and Compounds, 311(1), 33-39.

9. Ito, S., Matsui, H., Okada, K. I., Kusano, S. I., Kitamura, T., Wada, Y., & Yanagida, S. (2004). Calibration of solar simulator for evaluation of dye-sensitized solar cells. Solar energy materials and solar cells, 82(3), 421-429.

10. Eichhorn, K. (2006). LEDs in automotive lighting. In Light-Emitting Diodes: Research, Manufacturing, and Applications X. International Society for Optics and Photonics, 6134, 613405-1–6

11. NASA – Ion Propulsion https://www.nasa.gov/centers/glenn/about/fs21grc.html

12. Franks, N. P., Dickinson, R., De Sousa, S. L. M., Hall, N. A., & Lieb, W. R. (1998). How does xenon produce anaesthesia?. Nature, 396(6709), 324.

13. Van Eijk, C. W. (2002). Inorganic scintillators in medical imaging. Physics in Medicine & Biology, 47(8), R85.

14. Lachmann, B., Armbruster, S., Schairer, W. O. L. F. G. A. N. G., Landstra, M., Trouwborst, A., Van Daal, G. J., ... & Erdmann, W. (1990). Safety and efficacy of xenon in routine use as an inhalational anaesthetic. The Lancet, 335(8703), 1413-1415.

15. Sanders, R. D., Franks, N. P., & Maze, M. (2003). Xenon: no stranger to anaesthesia. British journal of anaesthesia, 91(5), 709-717.

16. Wanner, A. (2006). U.S. Patent Application No. 11/509,809.

17. Sayre, E. D. Commercial Value of Used Nuclear Fuel Reprocessed with Elements Separated, Purified and Reduced to Metals.

18. Boyum, B. M. (1971). An economic evaluation of the recovery of krypton and xenon from nuclear fuels reprocessing plants (Master's thesis, University of Arizona.).

19. Brunner, R., Haina, D., Landthaler, M., Waidelich, W., & Braun-Falco, O. (1986). Applications of laser light of low power density. Experimental and clinical investigations. In Therapeutic Photomedicine (pp. 111-116). Karger Publishers.

20. Severinghaus, J. P., Grachev, A., Luz, B., & Caillon, N. (2003). A method for precise measurement of argon 40/36 and krypton/argon ratios in trapped air in polar ice with

applications to past firn thickness and abrupt climate change in Greenland and at Siple Dome, Antarctica. Geochimica et Cosmochimica Acta, 67(3), 325-343.

21. Costello, S., Desmulliez, M. P., & McCracken, S. (2012). Review of test methods used for the measurement of hermeticity in packages containing small cavities. IEEE transactions on components, packaging and manufacturing technology, 2(3), 430-438.

22. Wanner, A. (2006). U.S. Patent Application No. 11/509,809.

23. Wu, T., Feng, X., Elsaidi, S. K., Thallapally, P. K., & Carreon, M. A. (2017). Zeolitic imidazolate Framework-8 (ZIF-8) membranes for Kr/Xe separation. Industrial & Engineering Chemistry Research, 56(6), 1682-1686.

24. Zhang, C., Lively, R. P., Zhang, K., Johnson, J. R., Karvan, O., & Koros, W. J. (2012). Unexpected molecular sieving properties of zeolitic imidazolate framework-8. The journal of physical chemistry letters, 3(16), 2130-2134. Chicago.

25. Li, J. R., Kuppler, R. J., & Zhou, H. C. (2009). Selective gas adsorption and separation in metal–organic frameworks. Chemical Society Reviews, 38(5), 1477-1504.

26. Wilson, S. T., Lok, B. M., & Flanigen, E. M. Crystalline Metallophosphate Compositions. U.S. Patent 4,310,440, 1982.

27. Simmen, A., McCusker, L. B., Baerlocher, C., & Meier, W. M. (1991). The structure determination and rietveld refinement of the aluminophosphate AlPO4-18. Zeolites, 11(7), 654-661.

28. Wu, T., Lucero, J., Zong, Z., Elsaidi, S. K., Thallapally, P. K., & Carreon, M. A. (2018). Microporous Crystalline Membranes for Kr/Xe Separation: Comparison between AlPO-18, SAPO-34, and ZIF-8. ACS Applied Nano Materials, 1(1), 463-470.

29. Feng, X., Zong, Z., Elsaidi, S. K., Jasinski, J. B., Krishna, R., Thallapally, P. K., & Carreon, M. A. (2016). Kr/Xe Separation over a Chabazite Zeolite Membrane. Journal of the American Chemical Society, 138(31), 9791-9794.

30. Bonin, K. D.; Kresin, V. V. Electric-Dipole Polarizabilities of Atoms, Molecules, and Clusters; World Scientific: Singapore River Edge, NJ, 1997.

31. Hye Kwon, Y., Kiang, C., Benjamin, E., Crawford, P., Nair, S., & Bhave, R. (2017). Krypton-xenon separation properties of SAPO-34 zeolite materials and membranes. AIChE Journal, 63(2), 761-769.

32. Kwon, Y. H., Min, B., Yang, S., Koh, D. Y., Bhave, R. R., & Nair, S. (2018). Ion-Exchanged SAPO-34 Membranes for Krypton–Xenon Separation: Control of Permeation Properties and Fabrication of Hollow Fiber Membranes. ACS Applied Materials & Interfaces, 10(7), 6361-6368.

33. Anderson, R.; Schweitzer, B.; Wu, T.; Carreon, M.A.; Gomez-Gualdron, D. (2018) Molecular simulation insights on Xe/Kr separation in a set of nanoporous crystalline membranes ACS Applied Materials & Interfaces 10, 582-592.

34. Wu, T., Lucero, J., Sinnwell, M., Thallapally, P. K., Carreon, M. A. (2018). Recovery of Xenon from Air over ZIF-8 Membranes, Chem Commun. 54 (65), 8976-8979.

35. Wu, T., Lucero, J., Crawford, J.M., Sinnwell, M., Thallapally, P. K., Carreon, M. A. (2019). SAPO-34 membranes for xenon capture from air. Journal of Membrane Science 573, 288-292

36. Jones, J.T.A; et. al; Cooper, A.I. (2011) Modular and predictable assembly of porous organic molecular crystals Nature, 474, 367.

37. Tozawa, T.; et. al.; Cooper. A.I. (2009) Porous Organic Cages, Nat. Mater. 8, 973.

38. Lucero, J.; Elsaidi, S.K.; Anderson, R.; Wu, T.; Gomez Gualdron, D.; Thallapally, P.K.; Carreon, M.A. (2018) Time Dependent Structural Evolution of Porous Organic Cage CC3", Crystal Growth & Design , 18, 2, 921-927.

39. Lucero, J.; Crawford, J.M.; Osuna, C.; Carreon, M.A. (2019) Solvothermal synthesis of porous organic cage CC3 in the presence of dimethylformamide as solvent, CrystEngComm 21, 34, 5039-5044.

40. Lucero, J.; Osuna, C.; Crawford, J.M. Carreon, MA (2019) Microwave Assisted Synthesis of Porous Organic Cages C3 and C2, CrystEngComm 21, 4534-4537.

41. Lucero, J.; Jasinski, J.B.; Song, M.; Li, D.; Liu, L.; Liu, J.; De Yoreo, J.; Thallapally, P.K. Carreon, M.A. (2019) Synthesis of Porous Organic Cage CC3 via Solvent Modulated Evaporation, Inorganica Chimica Acta , in press, DOI: 10.1016/j.ica.2019.119312.

42. Li, S.; Carreon, M.A.; Zhang, Y.; Funke, H.H.; Noble, R.D.; Falconer, J.L (2010) Scale-up of SAPO-34 membranes for CO_2/CH_4 separation. Journal of Membrane Science 352 (1-2), 7-13.